ELSEVIER

Journal of Membrane Science 192 (2001) 129–143

journal of MEMBRANE SCIENCE

www.elsevier.com/locate/memsci

Rotating reverse osmosis: a dynamic model for flux and rejection

Sangho Lee, Richard M. Lueptow*

Department of Mechanical Engineering, Northwestern University, Evanston, IL 60208, USA

Received 1 March 2001; received in revised form 1 May 2001; accepted 2 May 2001

Abstract

Reverse osmosis (RO) is a compact process for the removal of ionic and organic pollutants from contaminated water. However, flux decline and rejection deterioration due to concentration polarization and membrane fouling hinders the application of RO technology. In this study, a rotating cylindrical RO membrane is theoretically investigated as a novel method to reduce polarization and fouling. A dynamic model based on RO membrane transport incorporating concentration polarization is used to predict the performance of rotating RO system. Operating parameters such as rotational speed and transmembrane pressure play an important role in determining the flux and rejection in rotating RO. For a given geometry, a rotational speed sufficient to generate Taylor vortices in the annulus is essential to maintain high flux as well as high rejection. The flux and rejection were calculated for wide range of operating pressures and rotational speeds. © 2001 Elsevier Science B.V. All rights reserved.

Keywords: Concentration polarization; Reverse osmosis; Rotating filtration; Water treatment

1. Introduction

As water resources become more limited and waste discharge becomes increasingly problematic, the concept of wastewater recycling or water reuse is becoming important. Depending on the cost of water and wastewater treatment, the concept of water reuse is economically justified in many industries [1,2] including textiles [3], petrochemicals [4], food processing [5], pulp and paper [6], and tanning [7]. Another example of wastewater recycling is the wastewater management for manned space missions in which recycling of wastewater to produce potable water as well as water for washing will be essential to reduce the dependence on resupply of water [8–12]. In this case, mass, volume, and energy minimization are crucial [13].

Recently, reverse osmosis (RO) filtration has been considered a promising technology for water recycling and reuse. RO filtration removes ions and organic chemicals, and its treatment efficiency and performance are stable and predictable. RO processing has been successfully applied in wastewater recycling in several industries [14,15]. RO filtration has been shown to be adequate for producing clear water from recycled wastewater in various applications [16–18].

However, a problem that needs to be resolved in the application of RO membranes for wastewater recycling is the sensitivity to fouling, which results in a decrease in filtrate flux. Concentration polarization and subsequent membrane fouling are the most serious obstacles that limit the acceptance of RO membrane treatment. For example, with space mission wastewater, the potential for membrane fouling is high, since the wastewater contains large amounts of inorganic and organic solutes, pathogenic micro-organisms, and debris. Therefore, techniques to control membrane fouling are of great importance.

The reduction and alleviation of concentration polarization in filtration and RO have been the focus

* Corresponding author.
E-mail address: r-luetpow@northwestern.edu (R.M. Lueptow).

PII: S0376-7388(01)00493-8

Nomenclature

$C_{b,i}$	bulk concentration of solute (mol/m^3)
$C_{m,i}$	solute concentration at membrane surface (mol/m^3)
$C_{p,i}$	solute concentration at permeate side (mol/m^3)
d	annulus gap width ($=r_o - r_i$) (m)
D_i	solute diffusion coefficient (m^2/s)
J_{net}	net flux over time (m/s)
$J_{s,i}$	solute flux (mol/m^2 s)
$\bar{J}_{s,i}$	instantaneous flux for solute (m/s)
J_v	solvent flux (m/s)
$\bar{J}_v$	instantaneous flux for solvent (m/s)
k_i	mass transfer coefficient (m/s)
L	filter area length (m)
L_v	solvent transport parameter (m/s Pa)
$L_{s,i}$	solute transport parameter (m/s)
P_{loss}	pressure loss in rotating RO system (Pa)
ΔP_{axis}	pressure drop caused by axial flow in the annulus in rotating RO system (Pa)
ΔP_{rot}	pressure drop across the annulus gap in rotating RO system (Pa)
Q_{conc}	concentrate flow rate (m^3/s)
Q_{feed}	feed flow rate (m^3/s)
r_i	inner cylinder radius (m)
r_o	outer cylinder radius (m)
R	gas constant (J/mol K)
R_i	instantaneous rejection for solute
$R_{i,net}$	overall rejection over time
Re_a	axial Reynold number ($=2ud/\nu$)
REC	recovery
S_a	cross-sectional area of the annulus (m^2)
Sc_i	Schmidt number ($=\nu/D_i$)
t	time (s)
T	temperature (K)
Ta	Taylor number ($=r_i\omega d/\nu$)
Ta_c	critical Taylor number for a transition from stable Couette flow to vortical Taylor Couette flow
u	axial flow velocity (m/s)
x	position in axial direction (m)

Greek letters

η	radius ratio ($=r_i/r_o$)
ν	kinematic viscosity (m^2/s)
ρ	density (kg/m^3)
ω	rotational speed (s^{-1})
$\Delta\Pi_i$	osmotic pressure difference (Pa)

of much research and development [19]. Attempts to reduce concentration polarization include increasing the fluid velocity [20], inserting turbulence promoters in the feed channels [21], pulsing the feed flow over the membrane [22], and designing the flow path so Dean vortices occur [23,24]. High shear membrane filtration systems such as rotating disk membranes [25] and rotating cylinder filtration [26] have been also investigated because of their potential for reducing polarization.

Of particular interest in this paper is rotating filtration that takes advantage of centrifugal flow instabilities. Rotating filtration is relatively a new technique to control flux decline due to plugging of the filter pores during micro-filtration and ultra-filtration. The system consists of a cylindrical filter rotating within a stationary cylindrical shell. Toroidal Taylor vortices are induced by the rotation of the inner cylinder as a result of a centrifugal flow instability. The unique advantage of a rotating membrane filtration is that the build-up of particles and other species near the filter surface is very slow compared to dead-end or cross-flow filtration [27]. Many studies report a strong anti-fouling effect for rotating micro-filtration [28,29] and ultra-filtration [30]. Three mechanisms have been proposed for this resistance to fouling including Taylor vortices [31], centrifugal sedimentation of heavy particles [32], and shear due to the rotation [33]. Rotating filtration is presently used for the separation of plasma from whole blood [34,35] and other biological separations [31,36], but it also shows promise for a wide range of other applications. However, relatively little work has been done to further the application of rotating membrane filtration except for blood filtration [37]. Moreover, the use of a rotating system for reverse osmosis has not been investigated. Unlike micro-filtration there is no suspended species in the case of RO. Consequently, the critical issue is concentration polarization at the surface of the RO membrane rather than particles plugging the pores of the membrane.

In this paper, the implementation of rotating RO filtration for wastewater recovery is theoretically

investigated using combined transport models. Taking into consideration the complex time-dependent behaviors of filtration, the performance of rotating RO filtration is predicted as a function of module geometry, rotational speed, transmembrane pressure, axial flow rate, permeate velocity (flux), and feed composition. The optimum operating parameters are explored based on this approach. The analysis described here can be used for predicting rotating RO system performance for wastewater recovery and other potential industrial applications.

2. Modeling approach

We have applied the solution-diffusion model modified with the concentration polarization theory to predict rotating membrane performance over a wide range of conditions. Most previous studies using these equations only considered the steady-state behavior of filtration in simple geometries [38–40]. This paper extends this work in two ways. First, we include time-dependent behavior of the water flux and each solute component in the model. Second, we apply the model to the complex geometry of a rotating cylindrical RO membrane. In addition, the solution scheme has been improved over that used in our previous studies of a simpler system [18] to permit theoretical analysis of the effect of concentration polarization on the flux.

Fig. 1 shows the flow and geometry in a rotating RO membrane system. The solvent flux, $J_v(x, t)$, and the flux of solute component i, $J_{s,i}(x, t)$, through the inner cylinder membrane are [38]

$$J_v = L_v(\Delta P - P_{loss}) \tag{1}$$

$$J_{s,i} = J_v C_{p,i} = L_{s,i}(C_{m,i} - C_{p,i}) \tag{2}$$

where L_v and L_s are the solvent and solute transport parameters, $C_{m,i}(x, t)$ and $C_{p,i}(x, t)$ the solute concentrations at membrane surface and permeate side, ΔP the pressure difference from the device inlet to the permeate side of the membrane, and $P_{loss}(x, t)$ is the pressure loss by osmotic pressure and hydrodynamic effects in the annulus. P_{loss} in a rotating RO membrane system with axial flow includes four terms

$$P_{loss} = \sum_{i}^{n} \Delta\Pi_i + \Delta P_{rot} + \Delta P_{axis} + \rho g x \tag{3}$$

where $\Delta\Pi_i(x, t)$ is the osmotic pressure difference for solute i, ΔP_{rot} the pressure drop across the annulus gap in the rotating membrane module, ΔP_{axis} the pressure drop caused by axial flow in the annulus, and

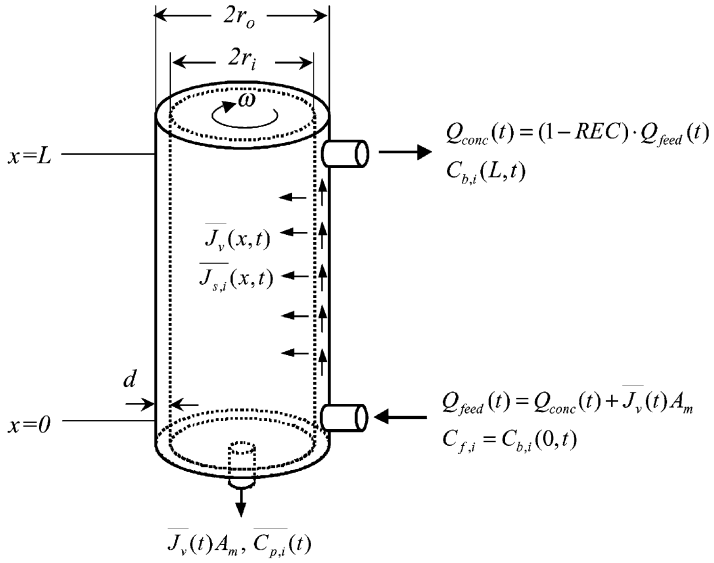

Fig. 1. Sketch of the flow and geometry in a rotating RO membrane system.

ρgx the hydrostatic pressure. The osmotic pressure is calculated by Van't Hoff's equation [41]

$$\Delta\Pi_i = (C_{m,i} - C_{p,i})RT \tag{4}$$

where R is the gas constant and T the temperature. The rotational pressure drop, P_{rot}, from the outer radius of the annulus (where fluid enters) to the inner radius of the annulus at the membrane is based on the solution of the Navier–Stokes equation for stable cylindrical Couette flow

$$\Delta P_{rot} = \rho\left[\frac{C_2^2}{2}\left(\frac{1}{r_i^2} - \frac{1}{r_o^2}\right) - \frac{C_1^2}{2}(r_i^2 - r_o^2) + 2C_1C_2\ln(\eta)\right] \tag{5}$$

where r_i is the inner cylinder radius, r_o the outer cylinder radius, ρ the density of the fluid, and $\eta = r_i/r_o$ the radius ratio. $C_1 = \omega(\eta^2/1-\eta^2)$ and $C_2 = \omega r_i^2(1/1-\eta^2)$ are parameters based on the rotational speed, ω, and the radius ratio. The pressure drop for laminar flow varies linearly with the axial position, so that the average pressure drop from the inlet to the outlet is expressed as [42]

$$\Delta P_{axis} = \frac{4\mu x u}{\{r_o^2 + r_i^2 - [(r_o^2 - r_i^2)/\ln(r_o/r_i)]\}^2} \tag{6}$$

where μ is the solvent viscosity, u the average axial flow velocity, and x the axial position in the module. For the conditions considered here, ΔP_{rot}, ΔP_{axis}, and ρgx are negligible compared to $\Delta\Pi_i$.

The difference between the solute concentration at the membrane, $C_{m,i}$, and the solute concentration in the bulk solution, $C_{b,i}$, originates from the concentration polarization phenomenon. On the basis of the film model theory and from Fick's law for diffusion, the concentration profile near the membrane surface is

$$\frac{C_{m,i} - C_{p,i}}{C_{b,i} - C_{p,i}} = e^{J_v/k_i} \tag{7}$$

where k_i is the mass transfer coefficient for the back diffusion of the solute i from the membrane to the bulk solution on high pressure side of membrane [43]. Rearranging Eq. (7), the solute concentration at the membrane surface ($C_{m,i}$) can be estimated from the solute concentration in the bulk phase, the permeate concentration, and the water flux. The growth of the concentration boundary layer is determined by the mass transfer coefficient, which in turn depends on the axial and rotational motion of the fluid. For axial flow, k_i depends on the axial Reynolds number $Re_a = 2ud/\nu$, where ν is the kinematic viscosity and $d = r_o - r_i$ the gap width. For rotational shear flow, k_i depends on the Taylor number (also known as the rotational Reynolds number), $Ta = r_i\omega d/\nu$. Above a critical Taylor number, Ta_c, toroidal vortices appear in the annular gap as a result of a centrifugal instability.

The mass transfer coefficient for laminar axial flow alone ($Ta = 0$, $Re_a > 0$), which is equivalent to cross-flow filtration, can be deduced from the Leveque equation. The Leveque solution for annular flow is [44]

$$k_i = 1.614 Re_a^{1/3} Sc_i^{1/3}\left(\frac{2d}{L}\right)^{1/3} \times \left(\left(\frac{\eta-1}{\eta}\right)\frac{\eta^2\ln\eta + (1-\eta^2)/2}{(1+\eta^2)\ln\eta + (1-\eta^2)}\right)^{1/3} \times \left(\frac{D_i}{2d}\right) \tag{8}$$

where D_i is the diffusion coefficient of solute i and $Sc_i = \nu/D_i$ the Schmidt number. In case of stable Couette flow (no vortices) in a rotating cylinder with negligible axial flow ($0 < Ta < Ta_c$, $Re_a \approx 0$), the analytical solution of mass transfer coefficient can be obtained. By rearranging the form given by Gabe and Robinson [45], the mass transfer coefficient for the stable Couette–Poiseuille flow is

$$k_i = 0.5510 Ta^{1/3} Sc_i^{1/3}\left(\frac{1+\eta^2}{1-\eta^2}\right)^{1/3} \times \left(\frac{1-\eta}{\eta}\right)^{-1/3}\left(\frac{D_i}{r_i}\right) \tag{9}$$

When the Taylor number exceeds a critical value (Ta_c), a transition from stable Couette flow to vortical Taylor–Couette flow occurs. An expression for Ta_c, modifying the form given by Murase et al. [26] to match the analytical result of Recktenwald et al. [46], is

$$Ta_c = 41.02\left(\frac{d}{r_i}\right)^{-0.5} + 25.75\left(\frac{d}{r_i}\right)^{0.5} + 1.85\left(\frac{d}{r_i}\right)^{1.5} \tag{10}$$

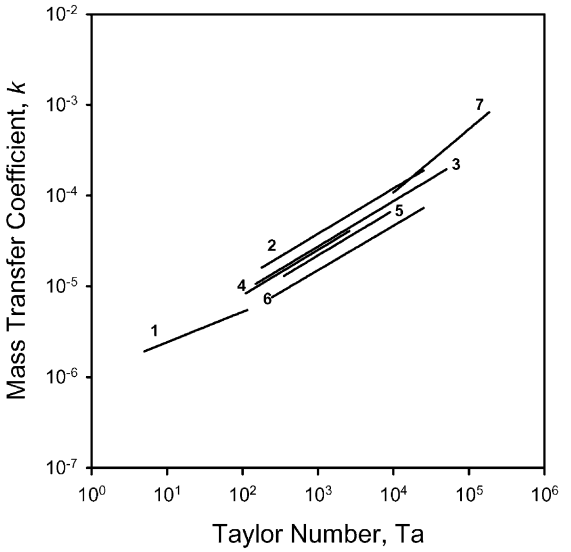

Fig. 2. Comparison of mass transfer correlations in the range of Taylor numbers considered. Inner cylinder radius, 0.0250 m; outer cylinder radius, 0.0286 m; solute, $(NH_4)_2CO_3$.

This expression matches the analytical value for Ta_c to within 0.5% over all η. There are several studies regarding the mass transfer in Taylor–Couette flow devices based on electrochemical methods [47–51], the Reynolds analogy [52], a theoretical model [53], a filtration method [54], and computational fluid dynamics [55]. But the differences among these published results are relatively small as shown in Fig. 2. In this study, we use the mass transfer expression of Holeschovsky and Cooney [54], which was obtained for a rotating ultra-filtration device, because it best matches the conditions that we intend to model. The mass transfer coefficient is

$$k_i = 1.4191 Ta^{1/2} Sc_i^{1/3} \left(\frac{1-\eta}{\eta}\right)^{0.42} \left(\frac{D_i}{2d}\right) \tag{11}$$

This expression is valid for $135 < Ta < 3700$, $Re_a < 200$, and $0.87 < \eta < 0.96$. In their experiments, the radial flow velocity was small enough to be neglected compared to axial and azimuthal velocities. We note that over this wide range of Taylor numbers a variety of vortical regimes can occur including non-wavy vortices, spiral vortices, wavy vortices, and so on [56,57]. However, in all cases, the secondary vortical flow enhances the mass transfer in a similar way, resulting in a single expression, Eq. (11), for the mass transfer coefficient.

During the filtration, J_v, $C_{b,i}$, and $C_{p,i}$ depend on axial position and time. From a mass balance of solute i, the time rate of change in $C_{b,i}$ in an annular fluid element is given by

$$\frac{\partial C_{b,i}(x,t)}{\partial t} = -\frac{1}{S_a}\left(Q_{conc}(t) + 2\pi r_i \int_x^L J_v(x,t)\,dx\right) \times \frac{\partial C_{b,i}(x,t)}{\partial x} + \frac{2\pi r_i J_v(x,t)}{S_a} C_{b,i}(x,t) - \frac{2\pi r_i J_{s,i}(x,t)}{S_a} \tag{12}$$

In Eq. (12), $S_a\pi(r_o^2 - r_i^2)$ is the cross-sectional area of the annulus, and Q_{conc} is the concentrate flow rate. The left hand side is the change in concentration of solute i in the fluid element. The first two terms on the right hand side are the changes in concentration due to axial flux of solute. The last term is the change in concentration due to the flux of solute through the membrane. This model does not account for flow effects near the inlet or outlet, which are negligible based on previous experience with rotating filtration devices [27–32]. The initial condition is that the bulk concentration in the annulus equals the constant inlet concentration so $C_{b,i}(x,0) = C_{b,i}(0,t) = C_{f,i}$. The system recovery is

$$\text{REC} = \frac{Q_{feed}(t) - Q_{conc}(t)}{Q_{feed}(t)} \tag{13}$$

where $Q_{feed}(t) = Q_{conc}(t) + 2\pi r_i L \bar{J}_v(t)$ and $\bar{J}_v(t)$ is defined shortly. In this work, $Q_{conc}(t)$ is assumed to be controlled by a feedback method to maintain constant recovery. Thus, $Q_{conc}(t)$ can be expressed as a function of permeate flux

$$Q_{conc}(t) = \frac{(1-\text{REC})2\pi r_i L \bar{J}_v(t)}{\text{REC}} \tag{14}$$

By simultaneously solving Eqs. (1)–(3), (7), and (12) for a given geometry, ω, ΔP, and REC, the flux and solute concentrations can be calculated as functions of time and axial position. The equations are solved using a fourth-order Runge–Kutta method. In Eqs. (1) and (2), L_v and L_s were obtained from experimental results for an low pressure reverse osmosis (LPRO) membrane [18].

Table 1
Composition of space mission wastewater [60][a]

Component	Concentration (mg/l)	Total nitrogen (mg/l)	Diffusion coefficient (m^2/s)	Solute permeability (m/s)
$(NH_4)_2CO_3$	3449.1	1006	1.42×10^{-9}	0.85×10^{-7}
NASA body soap[b]	190.6[c]	7.8	0.89×10^{-9}	0.34×10^{-7}
NaCl	1000	0	1.61×10^{-9}	1.60×10^{-7}

[a] Membrane parameters based on experiments using ESPA membrane [18]. Diffusion coefficients from [59].
[b] The detergent molecule in NASA body soap is $C_{15}H_{30}O_4NSNa$.
[c] Concentration is based on the net detergent concentration as linear alkylbenzene sulfonate (LAS).

After solving the set of equations, the spatially averaged flux is calculated by the integration of the solute concentration along the length of the filter

$$\bar{J}_v(t) = \frac{1}{L}\int_0^L J_v(x,t)\,dx \tag{15}$$

The net flux over time t is

$$J_{net} = \frac{1}{t}\int_0^t \bar{J}_v(t)\,dt \tag{16}$$

The instantaneous rejection for solute i is

$$R_i(t) = 1 - \frac{\bar{J}_{s,i}(t)}{(1/L)\int_0^L C_{b,i}(x,t)J_v(x,t)\,dx} \tag{17}$$

where $\bar{J}_{s,i}(t) = (1/L)\int_0^L J_{s,i}(x,t)\,dx$. The overall rejection over time is

$$R_{i,net} = 1 - \frac{(1/t)\int_0^t \bar{J}_{s,i}(t)\,dt}{C_{f,i}J_{net}} \tag{18}$$

3. Results and discussion

In this paper, we consider the application of rotating reverse osmosis for recycling space mission wastewater, which contains wash water, condensate, and urine. During storage, urea and other organic nitrogen compounds are converted to ammonium ions in the presence of urease from micro-organisms in the wastewater [58]. The simplified composition and properties of a synthetic model for space mission wastewater is given in Table 1 [59]. In addition to ammonium ions from urine, the wastewater contains NASA body soap and ions [60]. The solute permeabilities listed in Table 1 are based on our stirred cell measurements [18].

Consider first the results of a sample calculation. The geometric parameters in Table 2 that were used in the calculations are similar to those for a rotating reverse osmosis module that we are currently fabricating. All calculations are for room temperature operation. For these calculations the transmembrane pressure was 1800 kPa and the rotational speed was 200 rad/min. This corresponds to a Taylor number of 179, above the critical Taylor number for the appearance of vortical flow at this radius ratio. The net axial flow velocity was set to $u_{conc} = Q_{conc}/S_a = 0$ m/s. This, in effect, corresponds to "dynamic dead-end filtration", $Q_{conc}/Q_{feed} = 0$ and REC = 1.0. The solute concentration continually increases as filtration proceeds. However the rotation of the filter makes the system "dynamic" relative to the usual concept for dead-end filtration. Considering "dynamic dead-end filtration" is instructive in that it allows a simplified analysis without the complication of a net axial flow.

The flux and instantaneous rejection are shown in Fig. 3 as functions of time for dynamic dead-end filtration. Although the pure water flux of the membrane is 130 l/m^2 h, the permeate flux is substantially less because of the high osmotic pressure near the membrane.

Table 2
Parameters for the rotating RO membrane system[a]

Parameter	Value
Outer radius (r_o) (cm)	2.86
Inner radius (r_i) (cm)	2.50
Filter area length (L) (cm)	12.70
Annular gap (d) (cm)	0.36
Membrane area (A_m) (m^2)	0.0199
Water permeability (L_v) (m/s Pa)	2.00×10^{-11}
Kinematic viscosity (ν) (m^2/s)	0.98×10^{-6}

[a] Water permeability based on experiments using ESPA membranes [18].

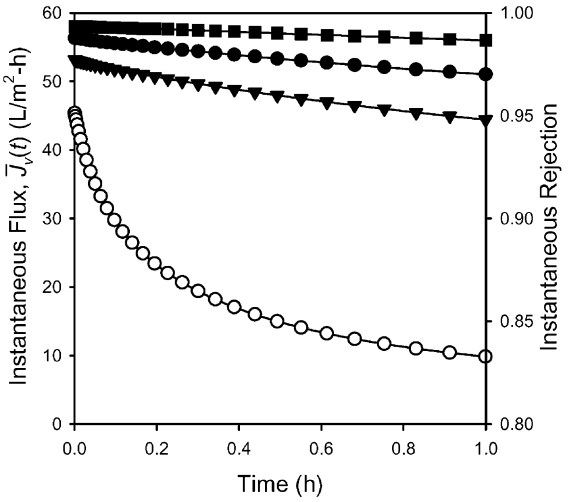

Fig. 3. Variation of permeate flux and rejection with time for space mission wastewater in a rotating RO system. Modeling condition: $\Delta P = 1800$ kPa; $\omega = 200$ rad/min ($Ta/Ta_c = 2.54$); REC = 1.0. (○) flux; (■) detergent rejection; (●) nitrogen rejection; (▼) NaCl rejection.

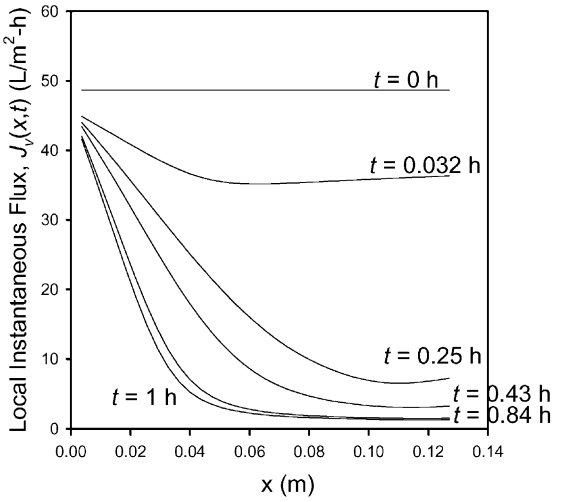

Fig. 4. Local flux of permeate as a function of time and position. Modeling condition: $\Delta P = 1800$ kPa; $\omega = 200$ rad/min ($Ta/Ta_c = 2.54$); REC = 1.0.

The flux decreases quite quickly as filtration proceeds because of the rapid increase in osmotic pressure as solute builds-up in the annulus. The instantaneous rejections for nitrogen (ammonium) and sodium chloride are initially high and decrease slightly with time. The rejection for detergent decreases less with time. It is important to note that the concentration factor, $f_c = V_f/V_c$ where V_f is the feed volume and V_c the concentrate volume, is quite large, about 5 after 1 h. For comparison, in a stirred cell with a concentration factor of only 2.5, the specific flux, $\bar{J}_v/\Delta P$, was less than 0.87×10^{-2} l/m^2 h kPa [18]. The specific flux at the same concentration factor in the rotating module is about 1.4×10^{-2} l/m^2 h kPa. This indicates how effective vortical motion in the rotating RO membrane system is in improving the flux.

The local permeate flux profiles for different times in dead-end filtration are shown in Fig. 4. Initially the flux is uniform, but the flux quickly drops off at the downstream end of the device because of the higher solute concentration there. The difference in flux between the upstream and downstream ends increases with increasing in time. It is evident that membrane fouling occurs first at the downstream end of the module because of the high solute concentration.

While it is helpful to consider dead-end filtration, a rotating RO system will likely operate with a net axial flow to carry the concentrate out of the system. Fig. 5 shows the dependence of flux and rejection on the fraction of the feed that passes through the membrane. The results are presented in terms of the recovery, REC, at different rotational speeds for 1 h of operation. A recovery of 1.0 corresponds to dead-end filtration; a recovery of 0.2 corresponds to 20% of the feed passing through the membrane. It is evident from Fig. 5(a) that the flux increases with rotational speed and decreases for high net recoveries. The dependence on rotational speed corresponds the increased mass transfer coefficient. At 0 rad/min, the mass transfer is quite low due to a lack of shear resulting in only a small flux through the membrane. At 70.8 rad/min, corresponding to $Ta/Ta_c = 0.9$, rotational shear enhances the mass transfer. At 86.5 rad/min, corresponding to $Ta/Ta_c = 1.1$, vortical motion results in additional shear and the transport of solute away from the membrane. This significantly increases the mass transfer and, consequently, the flux through the membrane. As the rotational speed is increased from 86.5 to 314.6 rad/min, the Taylor number is nearly quadrupled, resulting in a nearly doubling the mass transfer coefficient according to Eq. (11). At low recoveries, flux increases by more than two-thirds as Ta increases from 1.1 to

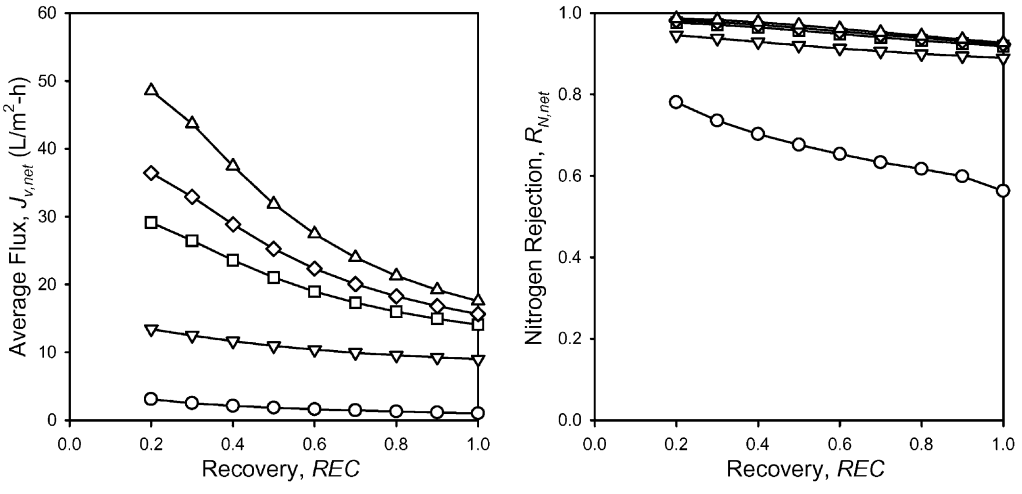

Fig. 5. Effect of recovery on permeate flux and nitrogen rejection in a rotating RO system. Modeling condition: $\Delta P = 1800$ kPa; operating time, 1 h. (a) Flux; (b) total nitrogen rejection. (○) $Ta/Ta_c = 0$ (0 rad/min); (▽) $Ta/Ta_c = 0.9$ (70.8 rad/min); (□) $Ta/Ta_c = 1.1$ (86.5 rad/min); (◇) $Ta/Ta_c = 2.0$ (157.3 rad/min); (△) $Ta/Ta_c = 4.0$ (314.6 rad/min).

4.0 Ta_c. However at high recoveries, the increase is substantially less (about 25%), although vortical flow results in significant higher flux than non-vortical flow. Of course, at all rotational speeds, the flux is highest for the lowest recovery. A low recovery corresponds to a high axial flow rate, Q_{conc}, that washes solute out of the device. The resulting lower solute concentration at the membrane permits a higher flux.

The rejection of total nitrogen, which is crucial in the application of space mission wastewater recovery, is nearly independent of the net recovery and the rotational speed, as shown in Fig. 5(b). The exception is 0 rad/min where solute builds up on the membrane surface because there is no fluid shear. The subsequent high concentration polarization results in solute passing through the membrane. Conditions above the critical Taylor number enhance rejection compared to $Ta/Ta_c = 0.9$, but the effect is small. Above the critical Taylor number, rejection is virtually unaffected by rotational speed. Thus, rotational speed enhances flux significantly, but has a relatively small effect on rejection. Similar results occur for the rejection of detergent and NaCl, so only nitrogen rejection is considered for the remainder of this paper.

Further insight into the effect of a net axial flow is evident in the permeate flux profiles at different times, shown in Fig. 6. At REC = 0.9, which is shown in Fig. 6(a), the local flux profiles are almost same as those in "dynamic dead-end" filtration shown in Fig. 4 because of the small net axial flow rate. As recovery decreases, the local flux is enhanced at the downstream end of the device compared to higher recoveries as shown in Fig. 6(b) for REC = 0.5. This is a consequence of the strong axial flow carrying solute out of the device. Of course, a practical rotating RO system would need to operate at relatively high recovery to minimize the concentrate volume. Consequently, for the remainder of this discussion we provide results for REC = 0.9.

The time-dependent variations in flux and nitrogen rejection are shown in Fig. 7 for several rotational speeds of the inner cylinder. Rotating RO has significant higher flux and rejection than no rotation which corresponds to a simple cross-flow system. The flux and rejection are higher for Taylor vortex flow ($Ta/Ta_c > 1$) than for circular Couette flow ($Ta/Ta_c = 0.9$) because of enhanced diffusion and mass transfer coefficient induced by the greater rotating shear flow and the Taylor vortices. The advantage of higher rotational speed diminishes as time progresses, although it remains far superior to cross-flow alone (0 rad/min). The rejection decreases only slightly as

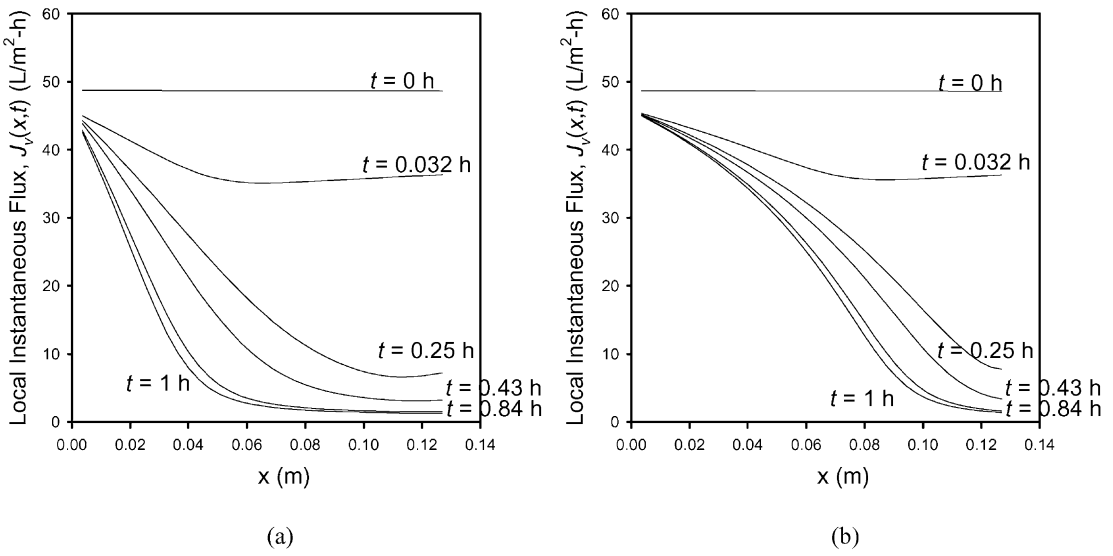

Fig. 6. Local flux of permeate as a function of time and position. Modeling condition: $\Delta P = 1800$ kPa; $\omega = 200$ rad/min ($Ta/Ta_c = 2.54$). (a) REC = 0.9; (b) REC = 0.5.

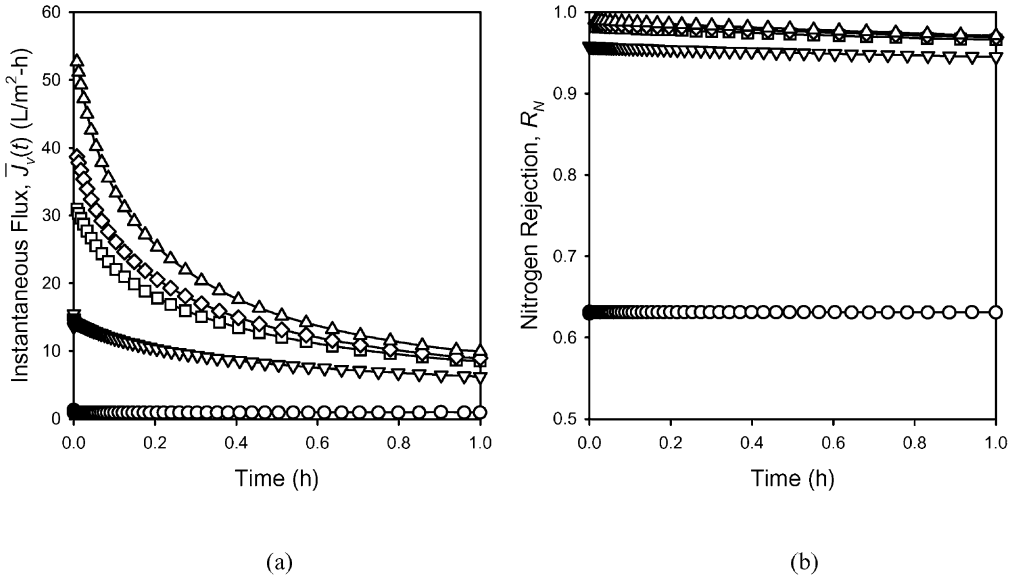

Fig. 7. Effect of rotational speed on permeate flux and total nitrogen rejection in a rotating RO system. Modeling condition: $\Delta P = 1800$ kPa; operating time, 1 h; REC = 0.9. (a) Flux; (b) total nitrogen rejection. (○) $Ta/Ta_c = 0$ (0 rad/min); (▽) $Ta/Ta_c = 0.9$ (70.8 rad/min); (□) $Ta/Ta_c = 1.1$ (86.5 rad/min); (◇) $Ta/Ta_c = 2.0$ (157.3 rad/min); (△) $Ta/Ta_c = 4.0$ (314.6 rad/min).

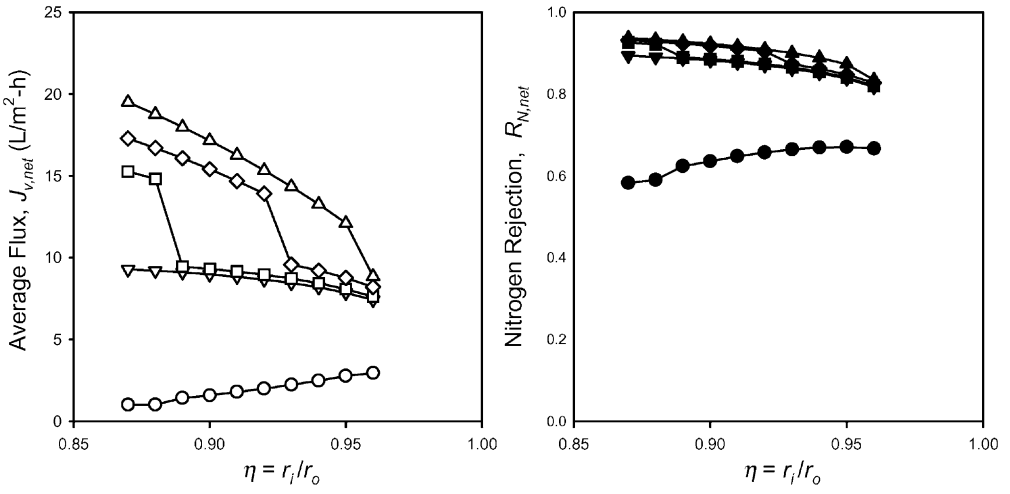

Fig. 8. Effect of radius ratio on flux and total nitrogen rejection in a rotating RO system. Modeling condition: $\Delta P = 1800$ kPa; REC = 0.9; operating time, 1 h. (a) Flux. (○) $Ta/Ta_c = 0$ (0 rad/min); (▽) $Ta/Ta_c = 0.9$ (70.8 rad/min); (□) $Ta/Ta_c = 1.1$ (86.5 rad/min); (◇) $Ta/Ta_c = 2.0$ (157.3 rad/min); (△) $Ta/Ta_c = 4.0$ (314.6 rad/min). (b) Total nitrogen rejection. (●) $Ta/Ta_c = 0$ (0 rad/min); (▼) $Ta/Ta_c = 0.9$ (70.8 rad/min); (■) $Ta/Ta_c = 1.1$ (86.5 rad/min); (◆) $Ta/Ta_c = 2.0$ (157.3 rad/min); (▲) $Ta/Ta_c = 4.0$ (314.6 rad/min).

time progresses. Again, the rejection with vortical flow ($Ta/Ta_c > 1$) is superior to cross-flow alone or non-vortical flow.

The geometry of the device would be expected to play a role in the effectiveness of rotating RO. A narrow gap (η near 1) would result not only in a high shear, but also in a higher critical Taylor number for the appearance of vortical flow. The dependence of permeate flux and nitrogen rejection over 1 h of operation on the radius ratio is shown in Fig. 8. To change η from 0.87 to 0.96, r_i is adjusted keeping r_o constant at 0.0286 m. The flux and rejection decrease with an increase in η except for 0 rad/min where the flux and rejection increase. For non-zero rotation, the results can be attributed to the dependence of annulus volume on η. Larger η results in a smaller annulus volume that makes rate of increase in concentration in the annulus faster leading to lower flux and rejection. At 0 rad/min, however, the annulus volume effect is negligible because of the high concentration polarization. Instead, an increase in η results in an increasing axial shear because of the narrower annular gap. This shear is negligible in dynamic filtration cases compared to the rotational shear. The sudden drops in flux for vortical flow (Ta/Ta_c of 1.1, 2.0 and 4.0) can be attributed to the stability of Taylor vortices. The critical Taylor number increases with increasing η. The sudden drops in flux correspond to the radius ratio at which the flow changes from vortical to non-vortical at that rotational speed. The magnitude of the drop in the flux is indicative of how important vortical flow is to enhancing the flux. A much smaller though noticeable drop is evident in the rejection at the same radius ratios.

The simulations to this point have been performed for a particular geometry of the rotating filter. A question that arises is the effect of the aspect ratio of the device on the performance, particularly in light of the significant axial variation in flux apparent in Fig. 6. The axial height of the filter and the radius of the inner cylinder can be varied while maintaining the filtration area and the radius ratio constant. The effect of aspect ratio, r_i/L, is shown in Fig. 9. The aspect ratio varies from 0.05 to 1.3 keeping the membrane filtration area at 0.0199 m^2. Regardless of changes in aspect ratio, flux and rejection are nearly the same when the rotational speed is held constant, as shown in Fig. 9(a). However, the flux decreases as aspect ratio increases when the Taylor number is held constant by adjusting the rotational speed accordingly, as shown in Fig. 9(b). This is because of the nature of

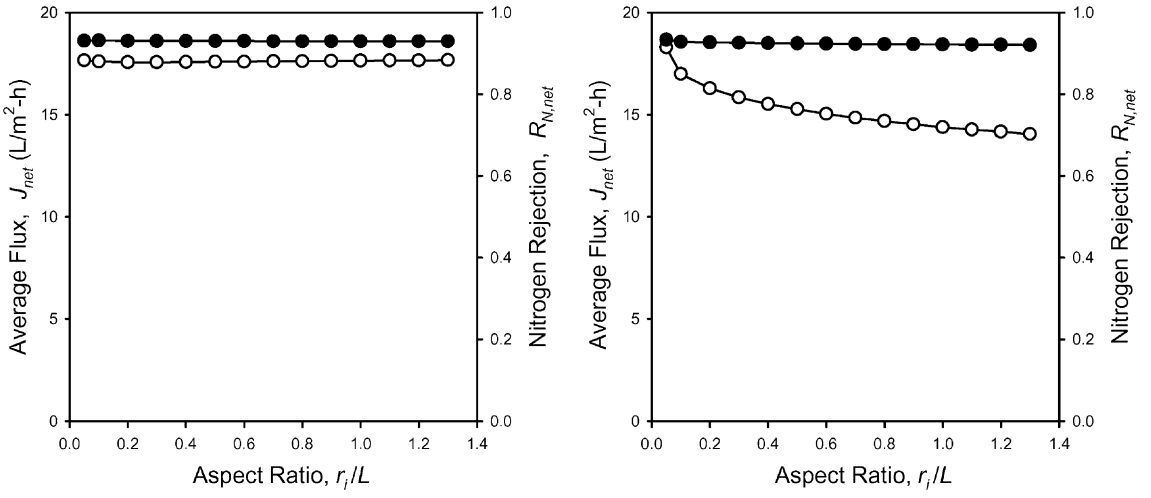

Fig. 9. Effect of aspect ratio on flux and total nitrogen rejection in a rotating RO system. Modeling condition: $\Delta P = 1800$ kPa; REC = 0.9; $\eta = 0.874$; membrane area, 0.0199 m^2; operating time, 1 h. Constant rotational speed, $\omega = 200$ rad/min ($1.66 < Ta/Ta_c < 4.29$) constant Taylor number, $Ta/Ta_c = 2.54$. (○) flux; (●) total nitrogen rejection.

the mass transfer coefficient in Taylor vortex flow. In Eq. (11), as r_i increases, Ta increases, but $(1-\eta)/\eta = d/r_i$ decreases. Since the exponents of two terms are similar, 0.5 and 0.42, respectively, the mass transfer coefficient changes very little when r_i is varied, accounting for Fig. 9(a). When Ta is constant, the mass transfer coefficient decreases as r_i increases because of $(1-\eta)/\eta$, which results in a net decrease in the permeate flux. In practice, the aspect ratio should be kept small anyway to optimize membrane area per unit volume of the apparatus, $2\pi r_i L/\pi r_i^2 L = 2/r_i$.

In addition to the geometric parameters of the module, membrane properties including solvent permeability and solute permeability play an important role in filtration performance. Fig. 10 illustrates how membrane properties affect permeate flux and nitrogen rejection. The flux increases as the solvent permeability increases (Fig. 10(a)), but the rejection is essentially unaffected by the solvent permeability. Increasing the solute (nitrogen) permeability results in an increase in the flux because of the lower osmotic pressure as solute passes through the membrane. Of course, there is also a significant decrease in rejection (Fig. 10(b)).

To further investigate the effect of operating conditions on the effectiveness of rotating RO membrane system, contours of constant flux and nitrogen rejection are shown as functions of rotational speed and transmembrane pressure in Fig. 11. The results are presented for 1 h of operation at 90% recovery. As expected, the best flux and rejection occur at high rotational speeds and high transmembrane pressures. However, dependence of flux and rejection on rotational speed and transmembrane pressure is not linear. The flux and rejection are suddenly increased at $\omega = 78$ because of the flow transition from stable Couette flow to Taylor vortex flow. For example, the flux in the non-vortical circular Couette flow regime is 7.66 l/m^2/h at 77.5 rad/min and 1400 kPa. A small increase of rotational speed results in a formation of vortices and increases the flux to 11.57 l/m^2/h at 78.5 rad/min. The flux increases somewhat with rotational speed as the enhanced mass transfer prevents the build-up of rejected species. However, the rejection increases only slightly with rotational speed once vortices appear.

An increase in the transmembrane pressure results in higher flux for both non-vortical circular Couette flow and Taylor vortex flow conditions, but the effect depends on the rotational speed. For example, the flux is about 5.35 l/m^2/h at 1000 kPa of transmembrane pressure and 50 rad/min. Doubling the transmembrane

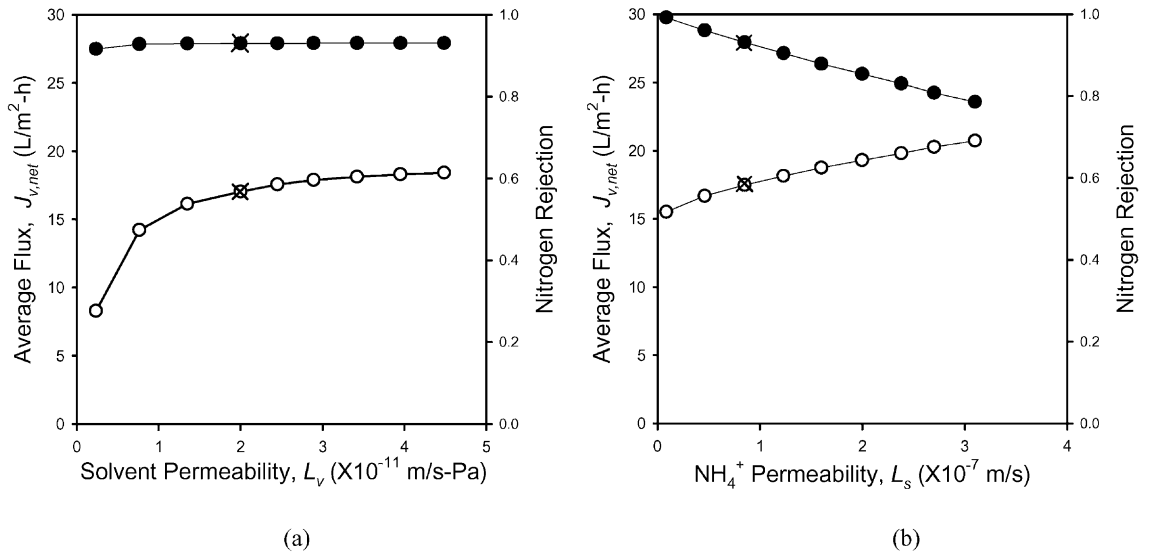

Fig. 10. Effect of membrane properties on flux and nitrogen rejection in a rotating RO system. Operating condition: $\Delta P = 1800$ kPa; $\omega = 200$ rad/min ($Ta/Ta_c = 2.54$); REC = 0.9; geometry as in Table 2. (a) Solvent permeability maintaining the solute permeabilities as in Table 1. (b) NH_4^+ permeability maintaining the other permeabilities as in Tables 1 and 2. (○) flux; (●) nitrogen rejection, (×) indicates permeabilities in Tables 1 and 2.

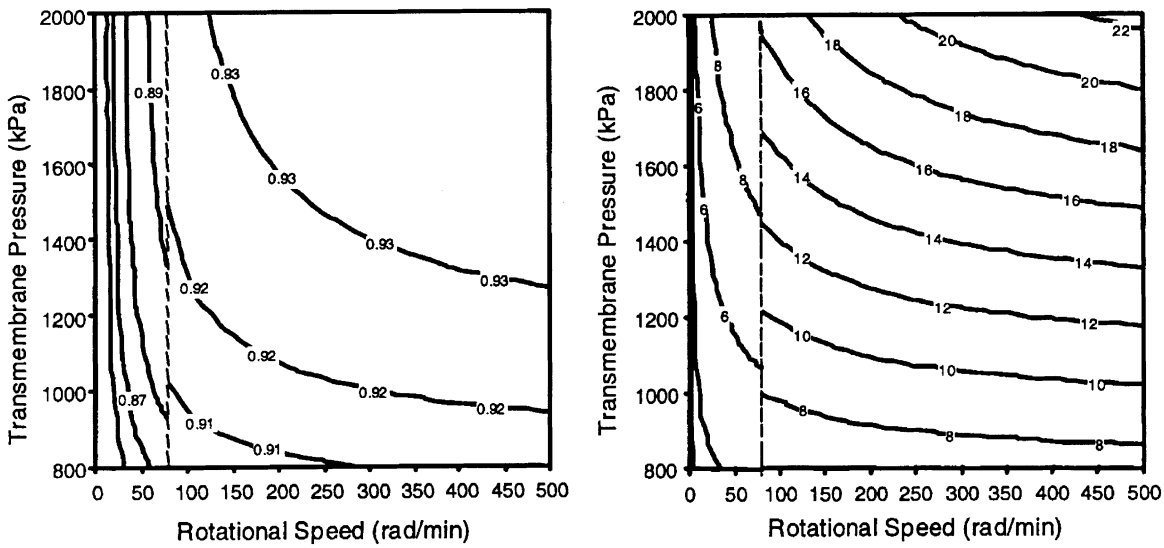

Fig. 11. Contour diagrams of net flux and total nitrogen rejection at different pressures and rotational speeds. Modeling condition: operating time, 1 h; REC = 0.9. (a) Average flux (l/m^2 h); (b) nitrogen rejection.

pressure increases the flux by 73%. Doubling the transmembrane pressure from 1000 to 2000 kPa at 100 rad/min increase the flux by 111%. Thus, increasing transmembrane pressure enhances flux more than increasing the rotational speed.

Nitrogen rejection depends on the operating conditions similarly to flux. However, the rejection is already quite high except for no rotation. When there is no rotation, the rejection is 0.6. The rejection increases to 0.83 when rotational speed is only 5 rad/min. In Taylor vortex regime, the rejection is about 0.9, only slightly better than for non-vortical operation. Similar results occur for NaCl and detergent rejections.

4. Conclusion

In this work, the flux and rejection for a rotating RO membrane system was theoretically predicted using a transient solution-diffusion model with concentration polarization and a mass transfer coefficient dependent on the Taylor number. The following conclusions can be drawn:

1. For a given geometry, a rotational speed sufficient to generate Taylor vortices in the annulus is essential to maintain high flux as well as high rejection. These vortices apparently reduce concentration polarization near the membrane and mix the solutes with the cross-flow fluid so they can be carried out of the device.
2. The recovery of the system affects the flux substantially. Flux is higher for the lowest recovery at all rotational speeds. Flux is enhanced much more by increasing rotational speed at low recoveries than at high recoveries, although vortical flow results in significantly higher flux than non-vortical flow in all cases.
3. The radius ratio (r_i/r_o) of the device plays a role in the effectiveness of rotating RO with a smaller radius ratios resulting in better flux and rejection. The sudden drops in the flux are predicted at radius ratios where the flow changes from vortical to non-vortical. This indicates how important vortical flow is to enhancing the flux. The rejection also decreases with increasing radius ratio, but the changes are much smaller than for the flux.
4. The aspect ratio (r_i/L) shows only negligible effect on the flux and rejection when the rotational speed is kept constant. However, at constant Taylor number, a smaller aspect ratio results in higher flux.
5. Flux increases with solvent permeability, but the rejection is essentially unaffected. Increasing the solute permeability results in an increase in flux, but it also causes a significant decrease in rejection.
6. Hydrodynamic operating conditions including transmembrane pressure and rotational speed greatly affect the flux and rejection. The best flux and rejection occur at high rotational speeds and high transmembrane pressures. Operating in Taylor vortex regime is most important to enhance the filtration performance. Flux and rejection increase slightly with rotational speed once vortices appear. Increasing transmembrane pressure significantly increases the flux.

Acknowledgements

This work was supported by NASA (Grant NAG9-1053), Karen Pickering, contract monitor.

References

[1] C.A. Buckley, C.J. Brouckaert, G.E. Rencken, Waste water reuse, the south African experience, Water Sci. Technol. 41 (10/11) (2000) 157–163.
[2] J. Lozier, Two approaches to indirect potable reuse using membrane technology, Water Sci. Technol. 41 (10/11) (2000) 149–156.
[3] A. Rozzi, F. Malpei, R. Bianchi, D. Mattioli, Pilot-scale membrane bioreactor and reverse osmosis studies for direct reuse of secondary textile effluents, Water Sci. Technol. 41 (2000) 189–195.
[4] J.M. Wong, Testing and implementation of an advanced wastewater reclamation and recycling system in a major petrochemical plant, Water Sci. Technol. 42 (5/6) (2000) 23–27.
[5] I. Koyuncu, M. Turan, D. Topacik, A. Ates, Application of low pressure nanofiltration membranes for the recovery and reuse of dairy industry effluents, Water Sci. Technol. 41 (1) (2000) 213–221.
[6] F. Yalcin, I. Koyuncu, I. Ozturk, D. Topacik, Pilot scale UF and RO studies on water reuse in corrugated board industry, Water Sci. Technol. 40 (4/5) (2000) 303–310.
[7] A. Cassano, R. Molinari, E. Drioli, Saving of water and chemicals in tanning industry by membrane processes, Water Sci. Technol. 40 (4/5) (2000) 443–450.
[8] NASA Lyndon B. Johnson Space Center, Advanced Life Support Program Requirements Definition and Design Considerations, CTSD-ADV-245 (REV A), Houston, Texas 77058, 1998.

[9] T.J. Salavin, M.W. Oleson, Technology trade-offs related to advanced mission wastewater processing, Waste Manage. Res. 9 (1991) 401–414.
[10] R.C. Cooper, The hygiene aspects of wastewater reuse, Waste Manage. Res. 9 (1991) 373–377.
[11] R.B. Dean, Processes for water reclaimation, Waste Manage. Res. 9 (1991) 425–430.
[12] A.D. Williams, C.S. Slater, Recovery of wastewater in microgravity (Space) applications using pervaporation processes and volatile rejection membranes, in: Proceedings of the Fifth International Conference on Pervaporation Processes, Bakish Materials Publishers, Englewood, NJ, 1991, pp. 383–391.
[13] D. Parker, ISS water reclamation system design, in: International Conference on Environmental Systems, July 1999, Denver, CO, USA, Session: International Space Station ECLSS I, System Aspects Water 1999-01-1950.
[14] D. Paul, K. Ohlrogge, Membrane separation processes for clean production, Environ. Progr. 17 (3) (1998) 137–213.
[15] D.J. Demboski, J.H. Benson, G.E. Rossi, N.S. Leavitt, M.A. Mull, Evolutions in U.S. navy shipboard sewage and graywater programs, in: Proceedings of the ASNE Environmental Symposium on Environmental Stewardship: Ships and Shorelines, November 1997.
[16] R.J. Ray, S.B. McCray, D.D. Newbold, Small-scale membrane systems for the recovery and purification of water, Sep. Sci. Technol. 26 (9) (1991) 1155–1176.
[17] S. Lee, R.M. Lueptow, Toward a reverse osmosis membrane system for recycling space mission wastewater, Life Support Bios. Sci. 7/3 (2001) 151–161.
[18] S. Lee, R.M. Lueptow, Reverse osmosis filtration for space mission wastewater: membrane properties and operating conditions, J. Membr. Sci. 182 (2001) 77–90.
[19] E. Matthiasson, B. Sivik, Concentration polarization and fouling, Desalination 35 (1980) 59–103.
[20] U. Merin, M. Cheryan, Factors effecting the mechanism of flux decline during ultra-filtration of cottage cheese whey, J. Food Proc. Pres. 4 (3) (1980) 183–198.
[21] W.F. Blatt, A. Dravid, A.S. Michaels, L. Nelson, Membrane Science and Technology, Plenum Press, New York, 1970, pp. 47–97.
[22] T.J. Kennedy, R.L. Merson, B.J. McCoy, Improving permeation flux by pulsed reverse osmosis, Chem. Eng. Sci. 29 (1974) 1927–1931.
[23] K.-Y. Chung, W.A. Edelstein, G. Belfort, Dean vortices with wall flux in a curved channel membrane system. Part 6. Two-dimensional magnetic resonance imaging of the velocity field in a curved impermeable slit, J. Membr. Sci. 81 (1993) 151–162.
[24] K.-Y. Chung, W.A. Edelstein, X. Li, G. Belfort, Dean vortices in a curved channel membrane system. Part 5. Three-dimensional magnetic resonance imaging and numerical analysis of the velocity field in a curved impermeable tube, AIChE J. 39 (10) (1993) 1592–1602.
[25] J. Engler, M.R. Wiesner, Particle fouling of a rotating membrane disk, Water Res. 34 (2) (2000) 557–565.
[26] T. Murase, E. Iritani, P. Chidphong, K. Kano, K. Atsumi, M. Shirato, High-speed micro-filtration using a rotating, cylindrical ceramic membrane, Ind. Chem. Eng. 31 (2) (1991) 370–378.
[27] R.M. Lueptow, Fluid mechanics of a rotating filter separator, in: K.J. Choi (Ed.), Advances in Filtration and Separation Technology, American Filtration and Separation Society, Vol. 9, North-port, AL, 1995, pp. 283–291.
[28] G. Belfort, J.M. Pimbley, A. Greiner, K.Y. Chung, Diagnosis of membrane fouling using a rotating annular filter. Part 1. Cell culture media, J. Membr. Sci. 77 (1993) 1–22.
[29] G. Belfort, P. Mikulasek, J.M. Pimbley, K.Y. Chung, Diagnosis of membrane fouling using a rotating annular filter. Part 2. Dilute particle suspensions of know particle size, J. Membr. Sci. 77 (1993) 23–39.
[30] F. Vigo, C. Uliana, Influence of the vorticity at the membrane surface on the performances of the ultra-filtration rotating module, Sep. Sci. Technol. 21 (4) (1986) 367–381.
[31] J.R. Hildebrandt, J.B. Saxton, The use of Taylor vortices in protein processing to enhance membrane filtration performance, in: R.C. Dean, R.M. Nerem (Eds.), Bioprocess Engineering Colloquium, ASME Book No. G00422 (1987).
[32] S.T. Wereley, R.M. Lueptow, Inertial particle motion in a Taylor–Couette rotating filter, Phys. Fluids 11 (2) (1999) 325–333.
[33] G. Belfort, R.H. Davis, A.L. Zydney, The Behavior of suspensions and macromolecular solutions in cross-flow micro-filtration, J. Membr. Sci. 96 (1994) 1–58.
[34] P. Perseghin, A. Pagani, P.M. Fornasari, L. Salvaneschi, Doonor plasmapheresis: a comparative study using four different types of equipment, Int. J. Artif. Organs. 10 (1987) 51–56.
[35] H. Fischel, W.F. McLaughlin, Blood fractionation system and method, US Patent 5,034,135 (1991).
[36] K.H. Kroner, V. Nissinen, Dynamic filtration of microbial suspensions using an axially rotating filter, J. Membr. Sci. 36 (1988) 85–100.
[37] L.J. Zeman, A.L. Zydney, Microfiltration and Ultrafiltration: Principles and Applications, Marcel Dekker, New York, 1996.
[38] C.S. Slater, C.A. Brooks III, Development of a simulation model predicting performance of reverse osmosis batch systems, Sep. Sci. Technol. 27 (11) (1992) 1361–1388.
[39] W.S.W. Ho, K.K. Sirkar, Membrane Handbook, Van Nostrand Reinhold, New York, 1992.
[40] J.G. Wijmans, R.W. Baker, The solution-diffusion model: a review, J. Membr. Sci. 107 (1995) 1–21.
[41] V.L. Snoeyink, D. Jenkins, Water Chemistry, Wiley, 1980.
[42] F.M. White, Fluid Mechanics, 3rd Edition, McGraw-Hill, Singapore, 1994.
[43] M. Cherayan, Ultra-filtration and Micro-filtration Handbook, Technomic Publishing Co. Inc., Lancaster, Basel, 1998.
[44] T.K. Ross, A.A. Wragg, Electrochemical mass transfer studies in annuli, Electrochim. Acta 10 (1965) 1093–1106.
[45] D.R. Gabe, D.J. Robinson, Mass transfer in a rotating cylinder cell. Part 1. Laminar flow, Electrochim. Acta 17 (1972) 1121–1127.
[46] A. Rectenwald, M. Lücke, H.W. Müller, Taylor vortex formation in axial through-flow: linear and weakly non-linear analysis, Phys. Rev. E 48 (6) (1993) 4444–4454.

[47] T. Mizushina, The electrochemical method in transport phenomena, Adv. Heat Transfer 7 (1971) 87–100.
[48] D.R. Gabe, D.J. Robinson, Mass transfer in a rotating cylinder cell. Part 2. Turbulent flow, Elecrochim. Acta 17 (1972) 1129–1137.
[49] K. Kataoka, H. Doi, T. Komai, Heat/mass transfer in Taylor vortex flow with constant axial flow rates, Int. J. Heat Mass Transfer 20 (1977) 57–67.
[50] F. Coeuret, J. Legrand, Mass transfer at the electrodes of concentric cylindrical reactors combining axial flow and rotation of the inner cylinder, Elecrochim. Acta 26 (7) (1981) 865–872.
[51] J. Grifoll, X. Farriol, F. Giralt, Mass transfer at smooth and rough surfaces in a circular Couette flow, Int. J. Heat Mass Transfer 29 (12) (1986) 1911–1918.
[52] D.A. Simmers, J.E.R. Coney, A Reynolds analogy solution for the heat transfer characteristics of combined Taylor vortex and axial flows, Int. J. Heat Mass Transfer 22 (1978) 679–689.
[53] Y. Kawase, J.J. Ulbrecht, Laminar mass transfer between concentric rotating cylinders in the presence of Taylor vortices, Electrochim. Acta 33 (2) (1988) 199–203.
[54] U.B. Holeschovsky, C.L. Cooney, Quantitative description of ultra-filtration in a rotating filtration device, AIChE J. 37 (8) (1991) 1219–1226.
[55] G. Baier, Liquid–liquid extraction based on a new flow pattern: two fluid Taylor–Couette flow computational fluid dynamics, Ph.D. Thesis, University of Wisconsin, USA, 1999.
[56] R.M. Lueptow, A. Docter, K. Min, Stability of axial flow in an annulus with a rotating inner cylinder, Phys. Fluids A 4 (1992) 2446–2455.
[57] S.T. Wereley, R.M. Lueptow, Spatio-temporal character of non-wavy and wavy Taylor–Couette flow, J. Fluid Mech. 364 (1998) 59–80.
[58] V.H. Varel, Use of urease inhibitors to control nitrogen loss from livestock waste, Bioresource Technol. 62 (1997) 11–17.
[59] D.R. Lide, CRC Handbook of Chemistry and Physics, CRC Press, Boca Raton, 2000.
[60] B.W. Finger, L.N. Supra, L. DallBauman, K.D. Pickering, Development and testing of membrane biological wastewater processors, in: Proceedings of the International Conference on Environmental Systems, SAE paper 1999-01-1947, 1999.